Original article

Nuclear Medicine Communications

A virtual sinogram method to reduce dental metallic implant artefacts in computed tomography-based attenuation correction for PET

Mehrsima Abdoli[a,b,e], Mohammad Reza Ay[a,b,c], Alireza Ahmadian[a,b] and Habib Zaidi[d]

Objective **Attenuation correction of PET data requires accurate determination of the attenuation map (μmap), which represents the spatial distribution of linear attenuation coefficients of different tissues at 511 keV. The presence of high-density metallic dental filling material in head and neck X-ray computed tomography (CT) scanning is known to generate streak artefacts in the resulting CT images and thus in the corresponding μmaps generated using CT-based attenuation correction. Consequently, an under/overestimation of activity concentration occurs in corresponding regions of the corrected PET images. The purpose of this study is to develop a simple yet practical approach for reduction of metallic dental implant artefacts in the generated μmaps.**

Methods **Currently available sinogram-based metal artefact reduction (MAR) algorithms operate directly on the raw sinograms. These usually consist of huge files stored in proprietary format not easily disclosed by the manufacturers and thus are not straightforward to read and manipulate. The proposed method uses the concept of virtual sinograms produced by forward projection of CT images in Dicom format for MAR. The projection data affected by metallic objects are detected in the sinogram space through segmentation of metallic objects in the CT image followed by forward projection of the metal-only image. Thereafter, the affected sinogram bins are replaced by interpolated values from adjacent projections using the spline interpolation technique. The algorithm was assessed using a polyethylene phantom containing materials simulating different tissues and a dedicated jaw phantom scanned before and after the insertion of metallic objects, where the corrected and noncorrected μmaps were compared with the artefact-free μmap. In addition, the Jaszczak and standard germanium phantoms including four metallic inserts were scanned on a PET/CT scanner to evaluate the impact of the MAR procedure on PET data through the comparison of uncorrected and corrected PET images to the actual activity concentrations in the phantoms. The proposed algorithm was also applied to head and neck CT images of 10 patients with metallic dental implants.**

Results **The MAR method proved to be practical in a clinical setting and reduced substantially the visible metal induced artefacts. The mean relative error in regions close to metallic objects is reduced by approximately 90%. The statistical analysis of the Jaszczak and solid Ge-68 phantoms PET images did not reveal statistically significant differences between the corrected and artefact-free images ($P > 0.05$). Moreover, the evaluation of clinical studies did not reveal statistically significant differences between the attenuation coefficients of the corrected μmaps and the expected theoretical values.**

Conclusion **The proposed MAR method provides a simple and convenient approach allowing correction for the presence of metal artefacts caused by dental implants without the need to manipulate the complex raw CT data. Further evaluation using a larger clinical PET/CT database is under way to evaluate the potential of the technique in a clinical setting.** *Nucl Med Commun* **31:22–31 © 2010 Wolters Kluwer Health | Lippincott Williams & Wilkins.**

Nuclear Medicine Communications 2010, **31**:22–31

Keywords: attenuation correction, attenuation map, metal artefacts, PET/CT, virtual sinogram

[a]Department of Medical Physics and Biomedical Engineering, School of Medicine, [b]Research Center for Science and Technology in Medicine, [c]Research Institute for Nuclear Medicine, Tehran University of Medical Sciences, Tehran, Iran, [d]Division of Nuclear Medicine, Geneva University Hospital, Geneva, Switzerland, and [e]Department of Nuclear Medicine and Molecular Imaging, University Medical Center Gronigen, University of Gronigen, Gronigen, Netherlands

Correspondence to Dr Mohammad Reza Ay, PhD, Department of Medical Physics and Biomedical Engineering, School of Medicine, Tehran University of Medical Sciences, Pour Sina Street, Tehran, Iran
Tel: +98 912 5789765; e-mail: mohammadreza_ay@tums.ac.ir

Received 5 March 2009 **Revised** 6 June 2009
Accepted 13 June 2009

Introduction

The introduction of dual-modality PET/computed tomography (CT) scanners combining the power of two complementary modalities to overcome the limitations of each technique alone is considered as one of the revolutionary technical advances that stimulated the wider clinical acceptance of molecular imaging [1]. Combining functional images with anatomic localization

0143-3636 © 2010 Wolters Kluwer Health | Lippincott Williams & Wilkins DOI: 10.1097/MNM.0b013e32832fa241

of metabolic abnormalities via hardware PET/CT image registration was shown to dramatically improve the potential of PET imaging for diagnosis, staging and restaging, assessment of response to therapy, surgery and treatment planning and prognosis assessment [2]. In addition, CT images can be utilized for attenuation correction (AC) of the corresponding PET data. The conversion procedure used for generating an attenuation map (μmap) from CT images involves three main steps: down sampling, energy mapping and smoothing. However, in the presence of highly attenuating objects (having a high atomic number), some dark and bright streaks appear in the reconstructed CT images. This is referred to as metal artefact, which is because of an inappropriate number of photons reaching the detectors. The most important cause of metal artefacts is beam hardening. Metallic implants such as hip prostheses, surgical clips and dental fillings induce this type of artefacts and lead to a discrepancy between reconstructed Hounsfield units and the actual attenuation coefficients. Hence the presence of metallic objects in the field-of-view of the CT scanner can lead to the wrong assessment of active abnormalities in the corresponding regions [3,4]. Although the less visible artefacts may not affect the visual quality of attenuation corrected PET images to a great extent [5], reduction of various sources of error and artefact will reduce the bias for the accurate quantification of PET data.

Metal artefact reduction (MAR) is essential to derive a reliable μmap for accurate CT-based attenuation correction (CTAC) of the PET data. Several techniques have been proposed for MAR [6]. These methods can be categorized in two main classes, namely sinogram-based and image-based methods. In sinogram-based methods, the correction procedure is implemented in sinogram space. Linear interpolation of the missing projection data belongs to this category of methods [7,8]. Because of the considerable difference between CT numbers of metallic objects and those of biological tissues, metallic objects can be easily segmented using simple thresholding techniques. The segmented image is then forward projected to estimate artificial projections, which are affected by metallic objects. These affected projections are then replaced by estimates derived by linear interpolation of neighbouring projection data along the same projection angle. Finally, the corrected CT image is reconstructed from the interpolated sinogram using the inverse radon transform. Cubic spline interpolation of unaffected projections is another way of replacing the missing projections [9]. Replacing missing projections by their unaffected correspondence is another method belonging to the same category of methods [10]. In this technique, instead of using an interpolation algorithm, the missing projections are replaced by their corresponding unaffected projections, that is, the opposite angular position in spiral scanning and the same angular position of the next slice in step scanning.

The second group of MAR methods operates in image rather than in sinogram space. Iterative deblurring [11], methods using wavelets [12,13], knowledge-based techniques [14], segmentation [15] and pattern recognition-based techniques [16] are some examples of methods belonging to this category. In these approaches, artefacts are treated as unwanted objects to be removed using enhancement methods. Obviously the degree of enhancement is limited to the accuracy of the applied algorithm. A precise detection of regions affected by metallic artefacts is a complicated task owing to the intrinsic ambiguities between CT numbers of artefacts and surrounding tissues.

The main challenge in implementing sinogram-based methods is the need to manipulate huge raw CT projection data, which are usually stored in manufacturer encrypted proprietary format. This makes the practical implementation of MAR algorithms exhausting and dependent on the scanner's brand. The aim of this study is to assess the performance and potential benefits of the virtual sinogram-based MAR method to generate artefact-free μmaps. It should be emphasized that this technique is not meant to generate metal artefact-free CT images of diagnostic quality, but rather to provide artefact-free μmaps suitable for accurate CTAC of the corresponding PET images.

Methods

Metal artefact reduction algorithm

The proposed method uses the concept of virtual sinograms for implementation of MAR, which are produced by forward projection of CT images in two-dimensional. This procedure is performed using a MATLAB (The MathWorks Inc., Natick, Massachusetts, USA) routine, which generates fan beam projection data from input images according to a predefined acquisition geometry. The geometry and projection parameters used in this procedure are similar to those of the scanner. The dimension of the sinogram matrix depends on the number of detectors and the difference (in degrees) between two successive steps of the forward projection process. These parameters were chosen to mimic those of the actual CT scanner.

Metallic objects present in CT images are segmented to allow detection of projection data affected by them in sinogram space. As the CT numbers (Hounsfield units) related to metallic objects are considerably higher than those of other tissues, image segmentation is performed using simple thresholding to extract a metal-only image (Fig. 1a and b). Thereafter this image is forward projected in 360° to obtain a sinogram corresponding to metallic objects. The same geometry and projection parameters are used in this procedure. In the obtained sinogram, sinogram bins associated with image pixels not affected

Fig. 1

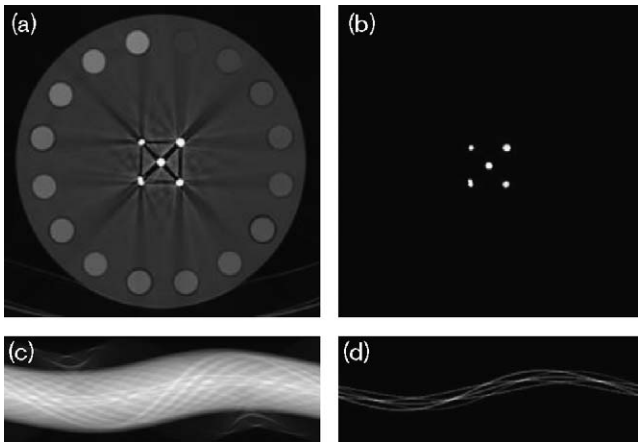

Detection of projections affected by metallic objects: (a) original computed tomography image, (b) metal only image, (c) original sinogram and (d) metal-only sinogram.

by metallic objects are assigned a nil value. Consequently, the pixels with intensities greater than zero reflect the sinogram bins affected by metallic objects (Fig. 1c and d) given that the sinogram bins are calculated from line integral of pixels they pass through.

The next step is to replace these sinogram bins in the original sinogram by appropriately scaled values. To do so, the affected sinogram bins are replaced by interpolated estimates from adjacent bins using the spline interpolation technique. Spline interpolation is a potent method to join discontinuous data, which uses polynomials to fit an appropriate curve to the whole data [17]. In comparison with other interpolation methods, splines result in the best replacement of missed projections in the corrected sinogram. The corrected sinogram is then reconstructed to generate an artefact-free CT image, which is then converted to a μmap as described above. The reconstruction algorithm used is based on a filtered back projection Matlab routine which utilizes the inverse radon transform where the elements of the sinogram matrix are backward projected to the image matrix. The reconstruction procedure assumes that the projections are collected for a fan-beam geometry. The obtained image matrix has the same size as the original CT image given that the same geometry and parameters are used by both forward and backward projection operators.

As described earlier, three steps are performed to produce the μmap from the corrected CT images. The first step consists in equalizing the size of the CT and PET images. This is achieved by down-sampling the corrected CT image by a factor of four. The linear attenuation coefficient measured with CT is calculated at the X-ray effective energy rather than at 511 keV. It is therefore necessary to convert linear attenuation coefficients of the CT scan to those corresponding to 511 keV in the second step [6,18]. In this study, a bilinear calibration curve is used for energy conversion, which is utilized by most commercial PET/CT scanners. The last step consists in matching the spatial resolution of the CT and PET images. A Gaussian filter with an appropriate kernel size is applied to the μmap to achieve this goal.

For the cylindrical polyethylene and jaw phantom studies, the μmap obtained without metallic inserts is compared with the μmap produced by the MAR corrected image. The comparison was performed by defining 28 regions of interest (ROIs) in different areas of the polyethylene phantom and 25 ROIs in different areas of the jaw phantom including teeth, bones, areas deteriorated by artefacts and artefact-free areas. The ROI statistics were analyzed for both the corrected and artefact-free images and the results reported on box and whisker plots. Likewise, reconstructed PET images of the Jaszczak phantom were assessed through comparison of the actual activity concentration within the phantom with the measured activity concentrations of 50 ROIs in the corrected PET images. A two-tailed paired *t*-test was used to assess statistically significant differences between the uncorrected/corrected images and artefact-free images acquired without metallic inserts.

For the clinical studies, in the absence of a gold standard for assessment, the resulting μmaps were analyzed by defining 25 ROIs in regions surrounding teeth and jawbone, which includes soft tissue. The calculated attenuation coefficients in these regions were compared with the expected theoretical attenuation coefficients of soft tissue at 511 keV using paired *t*-test statistical analysis.

Phantoms and scanning protocols

Four phantoms were used in this study to assess the performance of the proposed MAR algorithm through assessment of the generated μmaps and PET images. The first phantom is a 25 cm diameter cylindrical polyethylene phantom consisting of 16 syringes of 20 mm in diameter, filled with different concentrations of K_2HPO_4 solution to simulate different tissues of the human body, ranging form soft tissue to bone (Fig. 2). To simulate typical metallic artefacts in CT images, five metal inserts were placed in the middle of the phantom.

To assess the effect of metal streak artefacts caused by dental fillings on the accuracy of CTAC, a jaw phantom was designed and constructed. This 20 cm diameter phantom is made of a cylindrical plexiglas (4 cm in height) and consists of 16 syringes with different diameters filled with K_2HPO_4 solution with two different concentrations (Fig. 3). Eight and six syringes with diameters of 7 and

Fig. 2

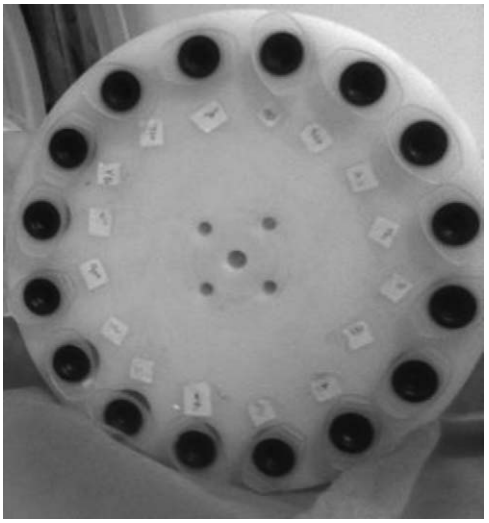

Photograph of the cylindrical polyethylene phantom consisting of 16 syringes filled with different concentrations of K_2HPO_4 solution simulating different biological tissues.

Fig. 3

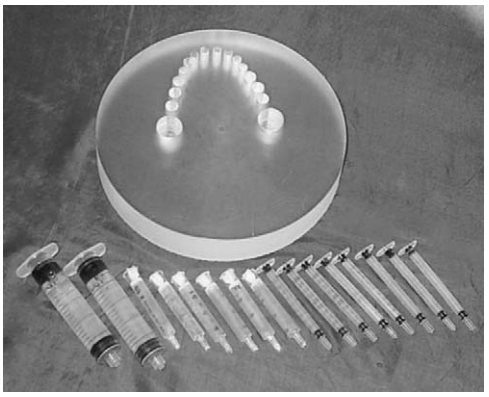

Photograph of the jaw phantom containing 16 syringes filled with different concentrations of K_2HPO_4 solution simulating teeth and jaw bone.

10 mm, respectively, were filled with a concentration of 1800 mg/cm^3 of K_2HPO_4 solution simulating teeth and two syringes with a diameter of 20 mm was filled with 900 mg/cm^3 concentration mimicking jaw bone. These inserts were arranged in a form that is approximately similar to a real jaw. To simulate metallic artefacts in CT images realistically, GK-110 dental amalgams manufactured by AT & M Biomaterials Co. Ltd. (Beijing, China), were inserted within the posterior teeth.

A clinical GE LightSpeed VCT 64 slice X-ray CT scanner (General Electric Healthcare Technologies, Waukesha, Wisconsin, USA) was used to scan the above-described phantoms. CT data were acquired twice (with and without metal inserts) in the same position using the same protocol used on the combined PET/CT system, namely 120 kV_p and 200 mAs. The scan without metallic inserts was performed to obtain an artefact-free image as a reference to which the MAR corrected images are compared. These phantoms were used to evaluate the μmaps generated from corrected CT images.

The Jaszczak phantom including metallic objects was also scanned on a PET/CT scanner to assess the impact of the MAR procedure on PET data through comparison of uncorrected and corrected PET images with the actual activity concentration in the phantom. The homogeneous compartment of the cylindrical phantom was filled with a mixture of fluorine-18 and water to reach an activity concentration of 16.67 kBq/cc. Four metallic inserts were placed inside the phantom to produce metallic artefacts. This experiment was performed only once in the presence of the metallic insertions owing to the fact that removing the insertions without phantom displacement was impracticable.

A solid cylindrical Ge-68 phantom having a volume of 6100 cc and an activity concentration of 8305.8 Bq/cc at scan time was also used for the assessment of the proposed algorithm. Four metallic rods were placed within the phantom to generate typical metal related artefacts. Similar to the previous experiment, the phantom was scanned only once in the presence of metallic rods.

The Jaszczak and solid Ge-68 phantoms were scanned on a Biograph 64-slice PET/CT scanner (Siemens Medical Solutions, Erlangen, Germany). The CT scan was performed at 120 kV_p and 160 mA, whereas the PET emission data was acquired during 40 min. The images were reconstructed using the attenuation weighted ordered subsets-expectation maximization (AW-OSEM) iterative reconstruction technique where both uncorrected and corrected CT images were applied for attenuation correction.

Clinical studies

CT images of 10 patients presenting with metallic dental implants were used. After the correction of these images, the corresponding μmaps were obtained and compared with expected theoretical attenuation coefficients of biological tissues in the absence of a gold standard. The mass attenuation coefficients of these tissues were calculated at 511 keV by means of the XCOM photon cross-section library [19] using human tissue composition data from ICRU 44 report [20]. The linear attenuation coefficients are then obtained by multiplying the mass attenuation coefficients by the density of the corresponding tissue.

It should be noted that, at this stage, our objective was to evaluate the performance of the algorithm in terms of artefact reduction achieved on μmaps obtained from clinical CT images. PET data of the Jaszczak phantom were also used to show that the correction of the μmap actually reduces the artefacts on the corresponding PET images. Application of the technique on clinical head and neck PET/CT data is ongoing; however, this prospective study will take time to collect a statistically relevant number of patients.

Results

The MAR algorithm was applied to CT images of the polyethylene and jaw phantoms containing metallic inserts followed by generation of the μmap (Figs 4 and 5). The MAR corrected CT images show substantial reduction of artefacts clearly visible on the original images. Likewise, the corresponding μmaps generated follow the same trend where only slight visible artefacts can be observed.

The quantitative analysis was performed using 28 ROIs defined on regions simulating different tissues of the human body and other regions including metal artefact in the polyethylene phantom. Likewise, 25 ROIs were defined on the jaw phantom in regions corresponding to jaw bones, posterior and anterior teeth, regions affected by artefacts inside the teeth, regions affected by artefacts outside the teeth and regions unaffected by artefacts. The same ROIs were also defined on the original, corrected and artefact-free μmap for both phantoms.

The mean values, standard deviations and standard errors for the ROIs defined on both the phantoms are reported in box and whisker plots to illustrate the relative difference between the original and the artefact-free μmaps (Fig. 6a and Fig. 7a) and between the MAR corrected and the artefact-free μmaps (Fig. 6b and Fig. 7b), respectively. As the results seem to suggest, the mean and standard deviation of the relative error are considerably reduced after the application of the MAR correction procedure.

The reconstructed CT and PET images of the Jaszczak and Ge-68 phantoms are illustrated in Figs 8 and 9, respectively. Metal artefacts observed on the uncorrected CT image give rise to typical metal related artefacts in the corresponding PET image (arrows in Fig. 8c and Fig. 9c). Table 1 summarizes the statistical analysis results of the Jaszczak and germanium phantoms. *P* values are obtained from a two-tailed paired *t*-test analysis to assess statistically significant differences between the uncorrected/corrected images and artefact-free images acquired without metallic inserts. The actual activity concentration and mean and standard deviations for 50 ROIs defined on the corrected PET images of the phantoms are also given.

The proposed algorithm was also applied to 10 clinical CT images presenting with metal dental implants. Figures 10 and 11 illustrate typical results showing MAR results on the CT images and the corresponding

Fig. 4

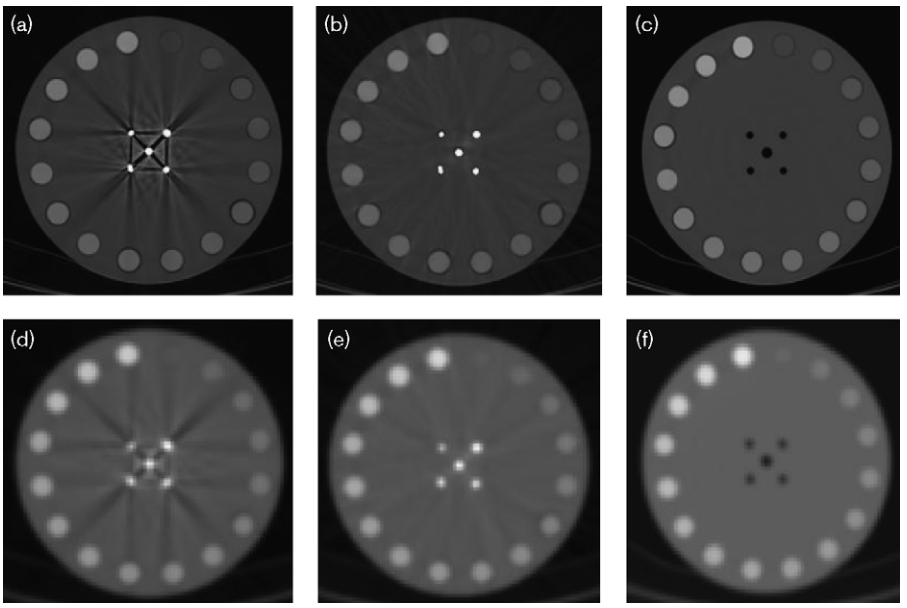

Computed tomography (CT) images and attenuation maps (μmaps) obtained for the polyethylene phantom. (a) Original CT image with metallic inserts, (b) metal artefact reduction corrected CT image, (c) original CT image without metallic inserts, (d) original μmap with metallic inserts, (e) MAR corrected μmap and (f) μmap without metallic inserts.

Fig. 5

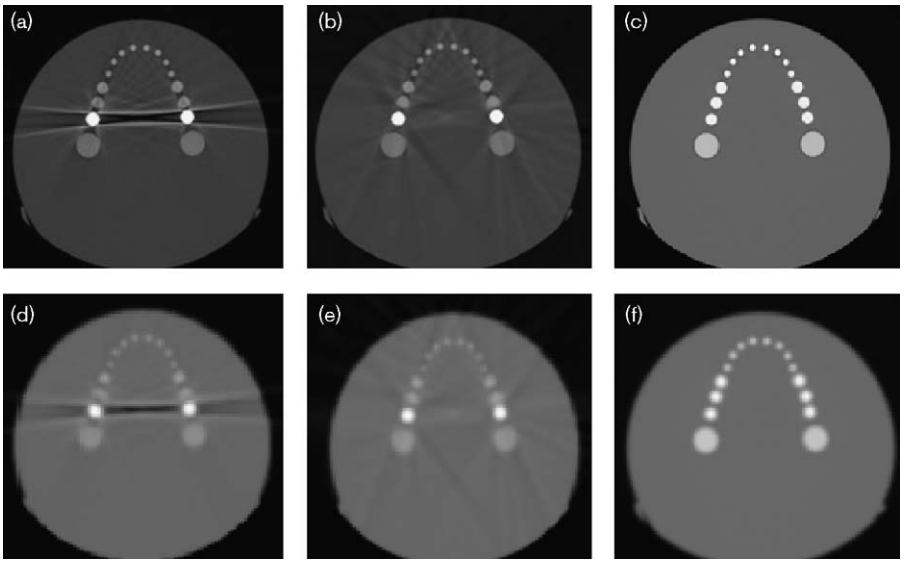

Computed tomography (CT) images and attenuation maps (μmaps) obtained for the jaw phantom. (a) Original CT image with metallic inserts, (b) metal artefact reduction (MAR) corrected CT image, (c) original CT image without metallic inserts, (d) original μmap with metallic inserts, (e) MAR corrected μmap and (f) μmap without metallic inserts.

Fig. 6

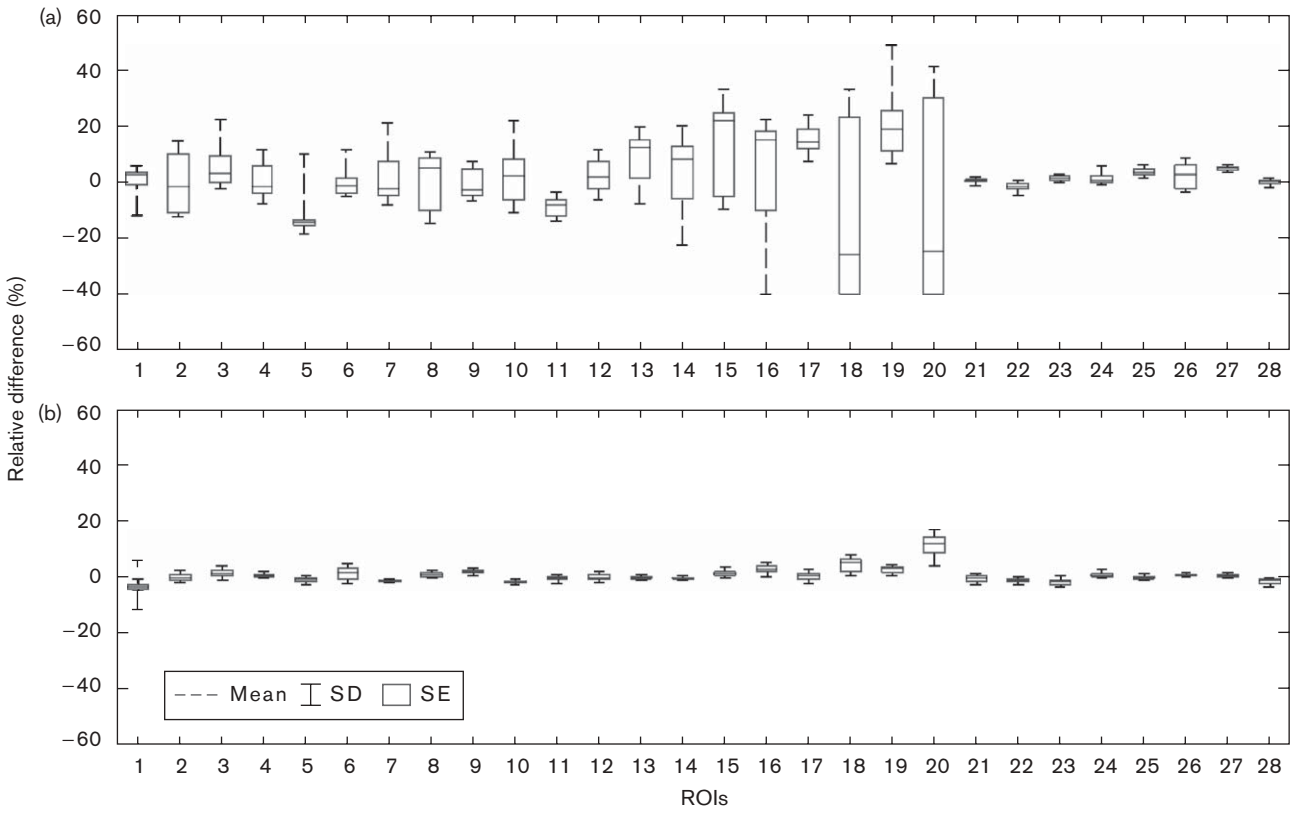

Box and whisker plots showing the relative difference for 28 regions of interest (ROIs) defined within the polyethylene phantom between the original attenuation maps (μmap) and the μmap obtained without metallic inserts (a) and between the metal artefact reduction corrected μmap and μmap obtained without metallic inserts (b). SD, standard deviation, SE, standard error.

Fig. 7

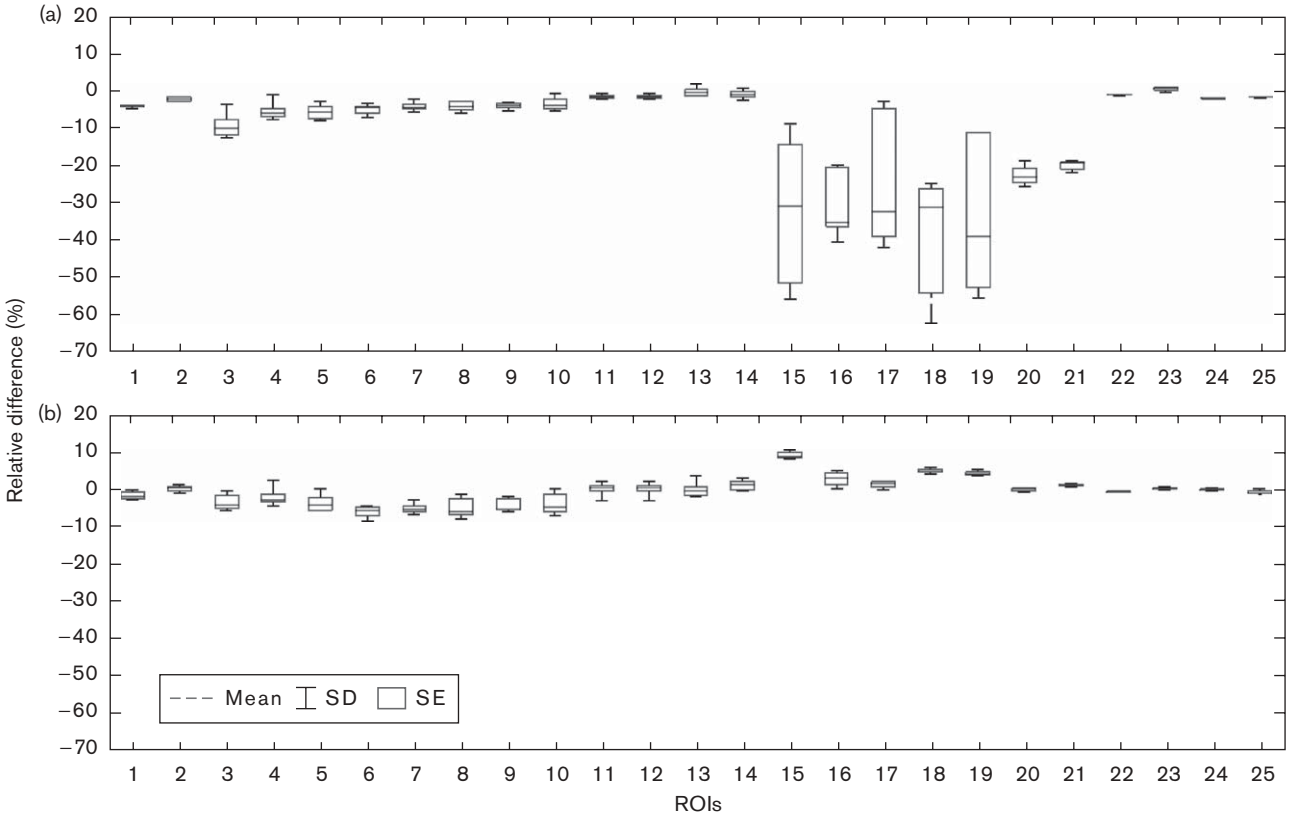

Box and whisker plots showing relative differences for 25 regions of interest (ROIs) defined within the jaw phantom between the original attenuation maps (μmap) and the μmap obtained without metallic inserts (a) and the metal artefact reduction corrected μmap and μmap obtained without metallic inserts (b). SD, standard deviation; SE, standard error.

μmaps for two patients. Although the proposed method does not produce a diagnostic quality CT image, the derived μmaps are of sufficient quality for AC purposes. The statistical analysis of the results obtained for all patients was performed using a paired *t*-test on the ROIs' estimates. Table 2 summarizes the mean values, standard deviations and *P* values resulting from the statistical analysis. The results did not reveal the existence of a statistically significant difference between calculated attenuation coefficients in the defined ROIs and the expected theoretical values at 511 keV.

Discussion

The progress in CTAC methodology has been immense in the last few years, the main opportunities arising from the development of both optimized scanning protocols and innovative and faster image processing algorithms. This has permitted the implementation of much more ambitious algorithms that tackle the challenges of whole-body imaging using PET. Some solutions were recently proposed and used successfully in clinical and research settings. This includes optimized contrast-enhanced CT protocols, respiratory motion compensation, metal artefacts reduction, truncation artefacts correction, beam hardening correction and X-ray scatter compensation in cone-beam CT [6].

Sinogram-based MAR algorithms inherently operate on the raw CT data to implement the correction procedure. These are huge files usually stored in encrypted proprietary format not generally disclosed by manufacturers and thus are not straightforward to handle or manipulate [21]. The proposed MAR algorithm has overcome these inconveniences using the virtual sinogram concept. Although CT images reconstructed from a virtual sinogram might not be of sufficient quality for clinical diagnosis, they are suitable for implementation of the CTAC procedure. One reason is that the CT images are downsampled and smoothed to match the resolution of PET images, which renders them less sensitive to small inaccuracies.

The experimental phantom and clinical results presented show that the proposed MAR method is suitable for generation of μmaps that can be used with confidence for AC of PET data using the CTAC procedure. It provides a simple and convenient method to correct

Fig. 8

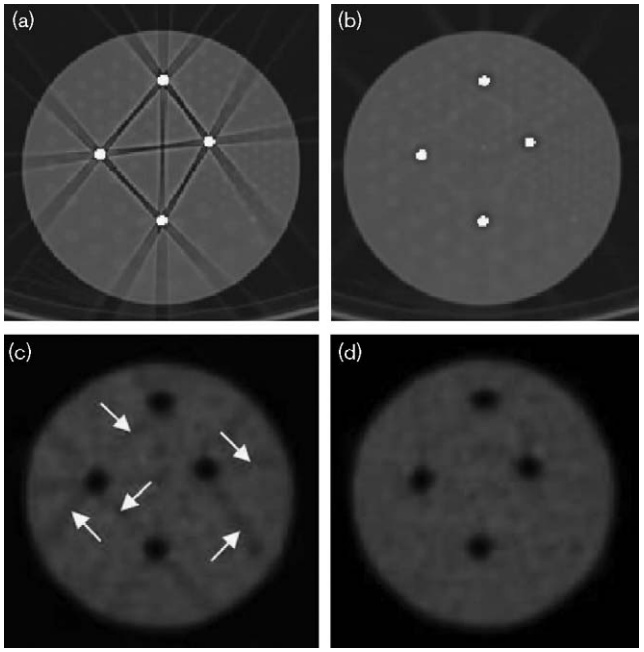

Representative slice of computed tomography (CT) and PET images of the Jaszczak phantom. (a) Original CT image, (b) corrected CT image using the metal artefact reduction algorithm, (c) original PET image corrected for attenuation using the CT images shown in (a) (arrows indicate the artefacts generated by the CT-based attenuation correction procedure), (d) PET image corrected for attenuation using the CT images shown in (b). Note the reduction of artefacts visible in (c).

Fig. 9

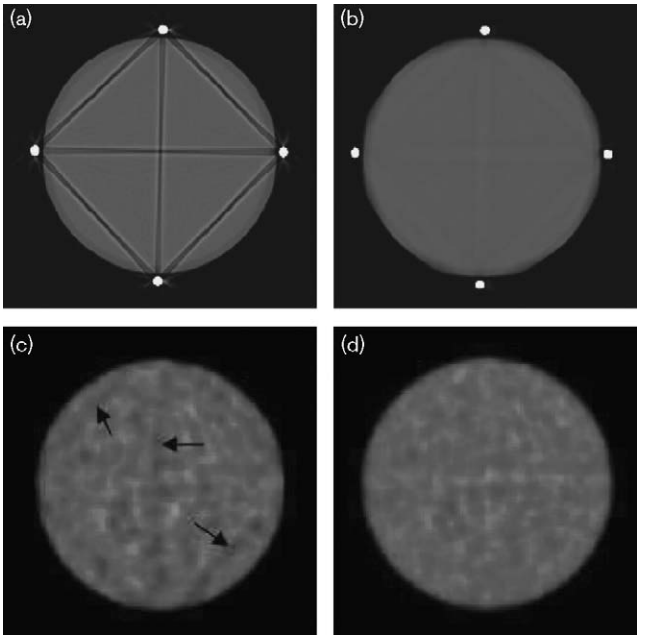

Representative slice of computed tomography (CT) and PET images of the Ge-68 solid phantom. (a) Original CT image, (b) corrected CT image using the MAR algorithm, (c) original PET image corrected for attenuation using the CT images shown in (a) (arrows indicate the artefacts generated by the CT-based attenuation correction procedure) and (d) PET image corrected for attenuation using the CT images shown in (b).

Table 1 Summary of statistical analysis results of uncorrected and corrected PET images using the MAR algorithm for both the Jaszczak and solid Ge-68 phantom study

Phantom	PET image	Mean ± SD (kBq/cc)	*P* value
Jaszczak phantom	Actual activity concentration	16.67	
	Corrected PET image	16.54 ± 0.64	0.098
	Uncorrected PET image	15.80 ± 0.79	<0.0001
Ge-68 solid phantom	Actual activity concentration	8.30	
	Corrected PET image	8.36 ± 0.34	0.131
	Uncorrected PET image	8.13 ± 0.34	<0.0001

MAR, metal artefact reduction; SD, standard deviation.

metallic artefacts caused by dental implants without the need to handle huge raw CT data by exploiting the potential of the virtual sinogram approach. The performance of the MAR algorithm for eliminating artefacts visible on the μmaps and PET images in regions adjacent to metallic objects is noticeable. As illustrated in Fig. 6a and Fig. 7a, the presence of metallic artefacts might cause a remarkable difference between the original μmap and the one obtained without metallic objects in some regions close to the location of the metallic object and between two metallic objects. It can be observed from Fig. 6b and Fig. 7b that these differences are considerably reduced using the proposed MAR approach. It should be noted that the errors did not change to a great extent in some regions, mostly those located in the regions unaffected by the artefacts.

The same observations can be made for the PET data obtained using the Jaszczak and Ge-68 phantoms. In the original uncorrected PET images, an underestimation of activity concentration can be observed owing to the dark streaks caused by metallic objects. After applying the MAR algorithm, the mean activity concentrations for the 50 selected ROIs are much closer to the actual ones (Table 1). Moreover, the standard deviation of ROIs inside the phantoms is reduced after the application of the MAR algorithm. Although the artefacts visible on both the phantoms are not strong enough to influence the visual quality of PET images and thus clinical diagnosis to a great extent, the quantitative analysis seems to suggest that reduction of these artefacts might reduce the bias when accurate quantitative analysis is desired.

Fig. 10

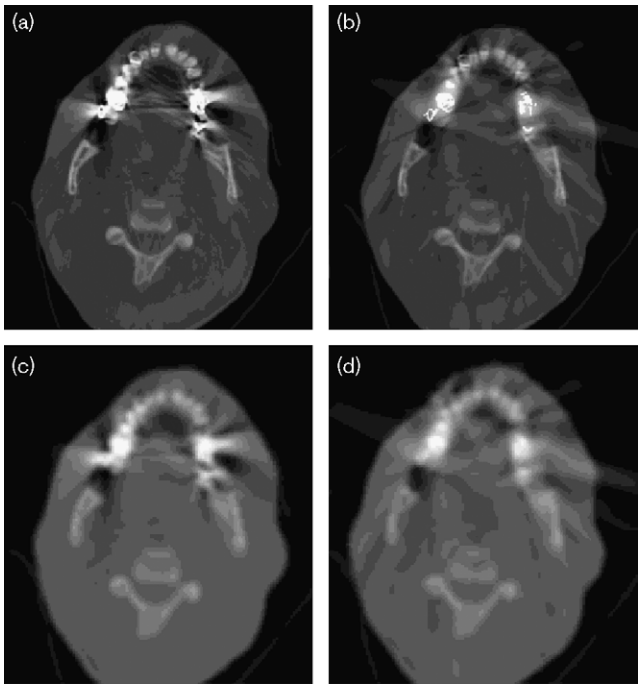

Typical slice through computed tomography (CT) images and attenuation maps (μmaps) for one clinical study showing (a) original CT image, (b) corrected CT image, (c) original μmap and (d) corrected μmap.

Fig. 11

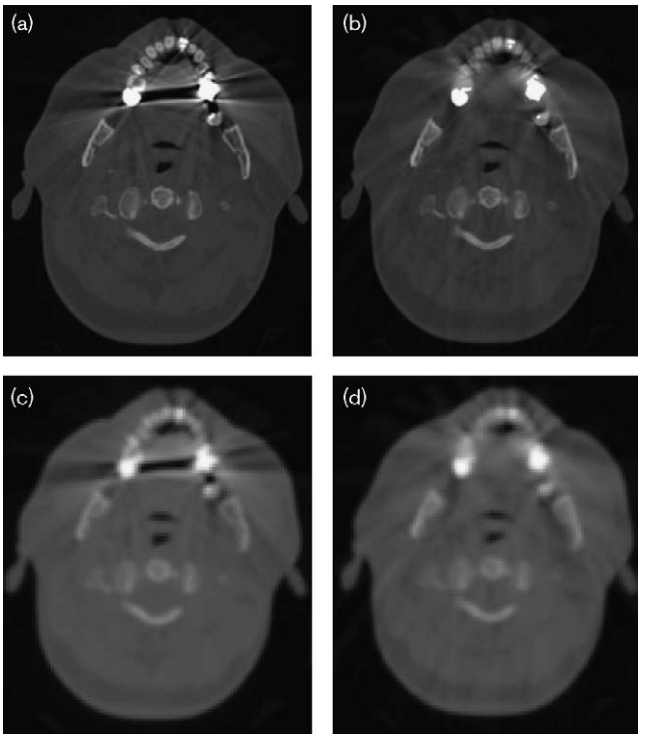

Typical slice through computed tomography (CT) images and attenuation maps (μmaps) for a second clinical study showing (a) original CT image, (b) corrected CT image, (c) original μmap and (d) corrected μmap.

Table 2 Summary of paired t-test analysis results for ROIs defined on patients' uncorrected and corrected μmaps in soft tissue regions

	Attenuation map					
	Uncorrected			Corrected		
Patient	LAC	SD	*P* value	LAC	SD	*P* value
1	0.106	0.036	0.028	0.091	0.004	0.052
2	0.110	0.045	0.002	0.091	0.004	0.099
3	0.110	0.036	0.007	0.091	0.003	0.060
4	0.109	0.038	0.016	0.092	0.007	0.057
5	0.111	0.038	0.007	0.093	0.008	0.055
6	0.111	0.035	0.003	0.091	0.006	0.128
7	0.109	0.036	0.008	0.091	0.003	0.056
8	0.110	0.038	0.012	0.091	0.003	0.127
9	0.110	0.037	0.007	0.091	0.003	0.103
10	0.112	0.041	0.008	0.091	0.004	0.160

The LAC of soft tissue is assumed to be equal to 0.096/cm.
LAC, linear attenuation coefficient; ROI, region of interest; SD, standard deviation.

In addition, the possibility to use a simple and fast MAR method is worth taking an extra step to obtain more accurate results.

In addition, successful application of the proposed MAR algorithm to clinical data seems to suggest that the technique can appropriately be used in clinical setting for MAR of μmaps generated from clinical CT images presenting with dental fillings and other metal related artefacts including prosthetic hips, chemotherapy ports, pacemakers, etc. As discussed earlier, this method is not aimed to produce diagnostic quality CT images, but reliable μmaps that can be used for AC. The next step of this study is to use the μmaps corrected by the proposed algorithm for AC of the clinical head and neck PET data, which is currently under way and will be reported in future publications.

Conclusion

A novel approach was proposed for reducing metal dental implant artefacts on CT images used in CTAC of PET data. The proposed method provides a simple and convenient approach allowing correction for the presence of metal artefacts without the need to manipulate the complex raw CT data. It can be concluded that the proposed method allows a substantial reduction of the strong artefacts located in regions adjacent to metallic objects in the generated μmap and thus the reconstructed PET images. The algorithm is being refined and further validated in a clinical setting using a larger clinical PET/CT database.

Acknowledgements

This study was supported by the Tehran University of Medical Sciences under the grant No. 132/494 and the Swiss National Science Foundation under the grant SNSF 3100A0-116547.

References

1 Townsend DW. Multimodality imaging of structure and function. *Phys Med Biol* 2008; **53**:R1–R39.
2 Kim JH, Czernin J, Allen-Auerbach MS, Halpern BS, Fueger BJ, Hecht JR, *et al*. Comparison between 18F-FDG PET, In-line PET/CT, and software fusion for restaging of recurrent colorectal cancer. *J Nucl Med* 2005; **46**:587–595.
3 Kamel EM, Burger C, Buck A, Schulthess GK, Goerres GW. Impact of metallic dental implants on CT-based attenuation correction in a combined PET/CT scanner. *Eur Radiol* 2003; **13**:724–728.
4 Lemmens C, Montandon M-L, Nuyts J, Ratib O, Dupont P, Zaidi H. Impact of metal artefacts due to EEG electrodes in brain PET/CT imaging. *Phys Med Biol* 2008; **53**:4417–4429.
5 Nahmias C, Lemmens C, Faul D, Carlson E, Long M, Blodgett T, *et al*. Does reducing CT artifacts from dental implants influence the PET interpretation in PET/CT studies of oral cancer and head and neck cancer? *J Nucl Med* 2008; **49**:1047–1052.
6 Zaidi H, Montandon M-L, Alavi A. Advances in attenuation correction techniques in PET. *PET Clin* 2007; **2**:191–217.
7 Kalender W, Hebel R, Ebersberger J. Reduction of CT artifacts caused by metallic implants. *Radiology* 1987; **164**:576–577.
8 Yazdi M, Gingras L, Beaulieu L. An adaptive approach to metal artifact reduction in helical computed tomography for radiation therapy treatment planning: experimental and clinical studies. *Int J Rad Oncol Biol Phys* 2005; **62**:1224–1231.
9 Bazalova M, Beaulieu L, Palefsky S, Verhaegen F. Correction of CT artifacts and its influence on Monte Carlo dose calculation. *Med Phys* 2007; **34**:2119–2132.
10 Yazdi M, Beaulieu L. A novel approach for reducing metal artifacts due to metallic dental implants. *IEEE Nucl Sci Symp Conf Rec* 2006; **4**:2260–2263.
11 Wang G, Snyder DL, O'Sullivan JA, Vannier MW. Iterative deblurring for CT metal artifact reduction. *IEEE Trans Med Imaging* 1996; **15**:657–664.
12 Zhao S, Robertson D, Wang G, Whiting B, Bae KT. X-ray CT metal artifact reduction using wavelets: an application for imaging total hip prostheses. *IEEE Trans Med Imaging* 2000; **19**:1238–1247.
13 Zhao S, Bae KT, Whiting B, Wang G. A wavelet method for metal artifact reduction with multiple metallic objects in the field of view. *J X-Ray Sci Technol* 2002; **10**:67–76.
14 Hamill JJ, Brunken RC, Bybel B, DiFilippo FP. A knowledge-based method for reducing attenuation artefacts caused by cardiac appliances in myocardial PET/CT. *Phys Med Biol* 2006; **51**:2901–2918.
15 Mirzaei S, Guerchaft M, Bonnier C, Knoll P, Doat M, Braeutigam P. Use of segmented CT transmission map to avoid metal artifacts in PET images by a PET-CT device. *BMC Nucl Med* 2005; **5**:3.
16 Kennedy JA, Israel O, Frenkel A, Bar-Shalom R, Azhari H. The reduction of artifacts due to metal hip implants in CT-attenuation corrected PET images from hybrid PET/CT scanners. *Med Biol Eng Comput* 2007; **45**:553–562.
17 Kincaid D, Cheney W. *Numerical analysis-mathematics of scientific computing*. 3rd ed. Boston: Brooks/Cole Publishing Company; 2002.
18 Kinahan PE, Townsend DW, Beyer T, Sashin D. Attenuation correction for a combined 3D PET/CT scanner. *Med Phys* 1998; **25**:2046–2053.
19 Berger MJ, Hubbell JH, Seltzer SM. XCOM: photon cross sections database. NBSIR 87-3597. Ionizing Radiation Division, Physics Laboratory, National Institute of Standards and Technology, Gaithersburg, MD 20899 NIST, Physics Laboratory, Office of Electronic Commerce in Scientific and Engineering Data, 1998.
20 Tissue Substitutes in Radiation Dosimetry and Measurement, ICRU Report No. 44, 1989.
21 Abdoli M, Ay MR, Ahmadian A, Sahba N, Zaidi H. *A novel approach for reducing dental filling artifact in CT-based attenuation correction of PET data. Proc. of the European Congress for Medical and Biological Engineering; Nov 23–27; Antwerp*. Belgium: Springer-Verlag Berlin Heidelberg; Vol. 22. 2008. pp. 492–495.